

Exceptional Points in a \mathcal{PT} -symmetrical quantum system: a Scattering matrix approach

J. Colín-Gálvez* and E. Castaño†

*Departamento de Física, Universidad Autónoma Metropolitana-Iztapalapa,
A. P. 55-534, 09340 Ciudad de México, Mexico.*

G. Báez‡

*Departamento de Ciencias Básicas, Universidad Autónoma Metropolitana-Azcapotzalco,
Av. San Pablo 420, Col. Nueva Rosario, 02128 Ciudad de México, Mexico.*

V. Domínguez-Rocha§

*Departamento de Ciencias Básicas, Universidad Autónoma Metropolitana-Azcapotzalco,
Av. San Pablo 420, Col. Nueva Rosario, 02128 Ciudad de México, Mexico and
Departamento de Física, Universidad Autónoma Metropolitana-Iztapalapa,
A. P. 55-534, 09340 Ciudad de México, Mexico.*

We analyze the behavior of a non-Hermitian opened one-dimensional quantum system with Parity-Time (\mathcal{PT}) symmetry. This system is built by a dimer, which has balanced gains and losses described by a parameter γ . By varying γ the system resonances, which are naturally separated, coalesce at the exceptional point (EP). The transmission spectrum is obtained by means of the scattering matrix (S matrix) formalism and we examine the wave functions corresponding to the resonances as a function of γ . Specifically, we look for the behavior and distribution of the phases of the S matrix before, at and after the exceptional point.

I. INTRODUCTION

Bender proposed in 1998 a new subset of non-Hermitian systems in which the energy spectrum has a real part¹. The Hamiltonians of this subset, which is called quasi-Hermitian, have the peculiarity of being invariant under the application of the symmetry operators of Parity, \mathcal{P} , and Time, \mathcal{T} . Also, regardless of whether this Hamiltonian is real or complex it has real eigenvalues^{2,3}. Systems with \mathcal{PT} -symmetry have a parameter associated with non-hermiticity that allows the transition between a real spectrum and a complex one. This transition was called Exceptional Point (EP) by Kato in 1966⁴. EPs appear when the variation of this parameter allows the coalescence of two naturally repelling eigenvalues, as well as their eigenvectors, of the associated Hamiltonian operator^{5,6}.

EPs arise when by varying a parameter associated with non-hermiticity, let us say γ , two or more eigenvalues coalesce. An example of a system with \mathcal{PT} -symmetry is a dimer made up of two coupled identical oscillators in which one of them has losses ($-i\gamma$) and the other one has gains ($+i\gamma$). The region prior to the critical value of the associated parameter ($0 \leq \gamma < \gamma_{EP}$) is known as the exact \mathcal{PT} -phase. In this region, the eigenvalues only have a real part. When the associated parameter reaches the critical value γ_{EP} , the eigenvalues and eigenvectors coalesce in EP. Exceeding the EP we arrive at a region called broken \mathcal{PT} -phase in which the imaginary part of the eigenvalue is different from zero. In the exact \mathcal{PT} -phase the system behaves as an Hermitian one, while in the broken \mathcal{PT} -phase the system reveals its non-Hermitian nature. EPs have been found in various areas of physics such as electromagnetism⁷, optics⁸, acoustics⁹, photonics¹⁰, elasticity¹¹, quantum mechanics¹², electronics¹³ or atomic physics¹⁴. EPs have been applied in improving the sensitivity of optical measurements⁸, in robust transfer of energy wireless¹³, in unidirectional invisibility¹⁴, in alteration of spectral bands^{15,16}, or in accelerometers¹⁷.

The system we study is made up of an open quantum dimer \mathcal{PT} -symmetric in one dimension. One of the scatterers of the dimer has losses while the other one has gains. Both losses and gains are balanced through a parameter associated with non-hermiticity. To study this system we use the formalism of the scattering matrix, or S matrix. In essence we will study the transmission spectrum of the system, the phase of the S matrix, its distribution, and the behavior of the wave function at resonances. These features will be analyzed as a function of γ before, at, and after the EP.

The following section presents the system under study as well as the analytic expressions for the S matrix. When varying the γ parameter an EP appears in the transmission spectrum. Thus we show the evolution of the real and imaginary parts of the wavefunctions associated to the coalescing resonances. We study the behaviour of the phase, and its distribution, in the subsequent section. Conclusions are presented at the end of this paper.

II. THE S MATRIX OF A SYSTEM WITH GAIN AND LOSSES

The system we are studying is a one-dimensional open quantum dimer with balanced gains and losses to which plane waves are incident from both sides. The dimer is made up of two scatterers whose real part of the potential that describes them is identical, while the signs of the imaginary part are opposite to each other. Each scatterer of the dimer is composed of three potential barriers as illustrated in Figure 1. The potential that describes the whole system is composed by seven regions. It is real for all regions except for regions III and V where the potential is complex. In regions I and VII the potential $V(x) = 0$; $V(x) = V_1$ for regions II (width c), IV (width b) and VI (width c); while the potential takes values $V_2 - i\gamma$ for region III (width a) (losses), and $V_2 + i\gamma$ for region V (width a) (gains). The width of the region IV is the sum of the barriers of each dimer scatterer since they are contiguous. For each of these regions the stationary solutions of the Schrödinger equation gives a superposition of plane waves traveling to the left and right given by $\psi_1(x) = a_1 e^{ik_1 x} + b_1 e^{-ik_1 x}$, and $\psi_i(x) = b_i e^{ik_i x} + a_i e^{-ik_i x}$ for $i = 2, 3, \dots, 7$. The wavenumbers are $k_1 = k_7 = \sqrt{2mE/\hbar^2}$, $k_2 = k_4 = k_6 = \sqrt{2m(E - V_1)/\hbar^2}$, $k_3 = \sqrt{2m[E - (V_2 - i\gamma)]/\hbar^2}$, and $k_5 = \sqrt{2m[E - (V_2 + i\gamma)]/\hbar^2}$, where m is the mass of the particle, while E is its energy ($V_1 > E > V_2$).

The scattering matrix relates amplitudes of the outgoing waves in terms of the incoming ones^{18,19}. In this case, the system has two opened channels²¹, thus the S matrix is of 2×2 and relates the amplitudes b_1 and b_7 in terms of the amplitudes a_1 and a_7 , namely

$$\begin{bmatrix} b_1 e^{ik_1(a+\frac{b}{2}+c)} \\ b_7 e^{ik_7(a+\frac{b}{2}+c)} \end{bmatrix} = S \begin{bmatrix} a_1 e^{-ik_1(a+\frac{b}{2}+c)} \\ a_7 e^{-ik_7(a+\frac{b}{2}+c)} \end{bmatrix}.$$

The S matrix has the form

$$S = \begin{bmatrix} r & t' \\ t & r' \end{bmatrix}, \quad (1)$$

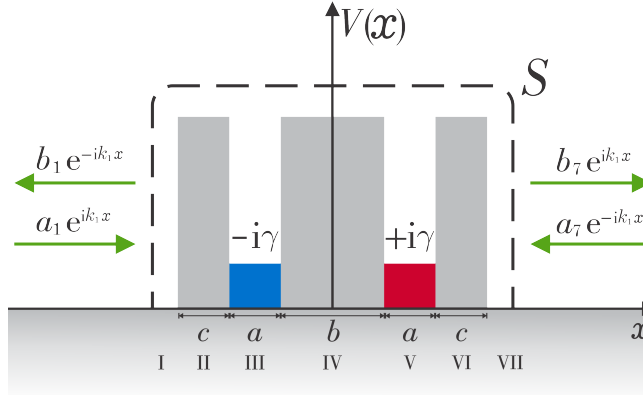


FIG. 1. Diagram of a dimer composed of two scatterers, with three potential barriers each one. The potential of the outer barriers of each scatterer is real, while the potential described by the central barrier is complex. The sign of the imaginary part of the central barrier gives rise to losses (represented in the blue region) or gains (represented in the red region). As expected, this system is quasi-Hermitian since it is invariant when applying the operators \mathcal{PT} .

where r and t (r' and t') are the amplitudes of reflection and transmission of the dimer when the waves are incident from the left (right). We must emphasize that the dependence of r, t, r' and t' on γ is implicit in the wavenumber. Explicitly these elements are

$$\begin{aligned}
r = & r_{12} + t'_{12} \frac{1}{e^{-2ik_1c} - r'_{12} r_{23}} r_{23} t_{12} + t'_{12} \frac{e^{-ik_1c}}{e^{-2ik_1c} - r'_{12} r_{23}} t'_{23} \frac{1}{e^{-2ik_2a} - r'_{1-3} r_{34}} r_{34} t_{23} \frac{e^{-ik_1c}}{e^{-2ik_1c} - r'_{12} r_{23}} t_{12} \\
& + t'_{12} \frac{e^{-ik_1c}}{e^{-2ik_1c} - r'_{12} r_{23}} t'_{23} \frac{e^{-ik_2a}}{e^{-2ik_2a} - r'_{1-3} r_{34}} t'_{34} \frac{1}{e^{-2ik_1b} - r'_{1-4} r_{45}} r_{45} t_{34} \frac{e^{-ik_2a}}{e^{-2ik_2a} - r'_{1-3} r_{34}} t_{23} \frac{e^{-ik_1c}}{e^{-2ik_1c} - r'_{12} r_{23}} t_{12} \\
& + t'_{12} \frac{e^{-ik_1c}}{e^{-2ik_1c} - r'_{12} r_{23}} t'_{23} \frac{e^{-ik_2a}}{e^{-2ik_2a} - r'_{1-3} r_{34}} t'_{34} \frac{e^{-ik_1b}}{e^{-2ik_1b} - r'_{1-4} r_{45}} t'_{45} \frac{1}{e^{-2ik_2a} - r'_{1-5} r_{56}} r_{56} \\
& \times t_{45} \frac{e^{-ik_1b}}{e^{-2ik_1b} - r'_{1-4} r_{45}} t_{34} \frac{e^{-ik_2a}}{e^{-2ik_2a} - r'_{1-3} r_{34}} t_{23} \frac{e^{-ik_1c}}{e^{-2ik_1c} - r'_{12} r_{23}} t_{12} \\
& + t'_{12} \frac{e^{-ik_1c}}{e^{-2ik_1c} - r'_{12} r_{23}} t'_{23} \frac{e^{-ik_2a}}{e^{-2ik_2a} - r'_{1-3} r_{34}} t'_{34} \frac{e^{-ik_1b}}{e^{-2ik_1b} - r'_{1-4} r_{45}} t'_{45} \frac{e^{-ik_2a}}{e^{-2ik_2a} - r'_{1-5} r_{56}} \\
& \times t'_{56} \frac{1}{e^{-2ik_1c} - r'_{1-6} r_{67}} r_{67} t_{56} \frac{e^{-ik_2a}}{e^{-2ik_2a} - r'_{1-5} r_{56}} t_{45} \frac{e^{-ik_1b}}{e^{-2ik_1b} - r'_{1-4} r_{45}} t_{34} \frac{e^{-ik_2a}}{e^{-2ik_2a} - r'_{1-3} r_{34}} t_{23} \frac{e^{-ik_1c}}{e^{-2ik_1c} - r'_{12} r_{23}} t_{12}, \tag{2}
\end{aligned}$$

$$t = t_{67} \frac{e^{-ik_1c}}{e^{-2ik_1c} - r'_{1-5} r_{67}} t_{56} \frac{e^{-ik_2a}}{e^{-2ik_2a} - r'_{1-4} r_{56}} t_{45} \frac{e^{-ik_1b}}{e^{-2ik_1b} - r'_{1-3} r_{45}} t_{34} \frac{e^{-ik_2a}}{e^{-2ik_2a} - r'_{1-2} r_{34}} t_{23} \frac{e^{-ik_1c}}{e^{-2ik_1c} - r'_{12} r_{23}} t_{12}, \tag{3}$$

$$\begin{aligned}
r' = & r'_{67} + t_{67} \frac{1}{e^{-2ik_1c} - r'_{56} r_{67}} r'_{56} t'_{67} + t_{67} \frac{e^{-ik_1c}}{e^{-2ik_1c} - r'_{56} r_{67}} t_{56} \frac{1}{e^{-2ik_2a} - r'_{45} r_{7-5}} r'_{45} t'_{56} \frac{e^{-ik_1c}}{e^{-2ik_1c} - r'_{67} r'_{56}} t'_{67} \\
& + t_{67} \frac{e^{-ik_1c}}{e^{-2ik_1c} - r'_{56} r_{67}} t_{56} \frac{e^{-ik_2a}}{e^{-2ik_2a} - r'_{45} r_{7-5}} t_{45} \frac{1}{e^{-2ik_1b} - r'_{34} r_{7-4}} r'_{34} t'_{45} \frac{e^{-ik_2a}}{e^{-2ik_2a} - r'_{45} r_{7-5}} t'_{56} \frac{e^{-ik_1c}}{e^{-2ik_1c} - r'_{56} r_{67}} t'_{67} \\
& + t_{67} \frac{e^{-ik_1c}}{e^{-2ik_1c} - r'_{56} r_{67}} t_{56} \frac{e^{-ik_2a}}{e^{-2ik_2a} - r'_{45} r_{7-5}} t_{45} \frac{e^{-ik_1b}}{e^{-2ik_1b} - r'_{34} r_{7-4}} t_{34} \frac{1}{e^{-2ik_2a} - r'_{23} r_{7-3}} r'_{23} \\
& \times t'_{34} \frac{e^{-ik_1b}}{e^{-2ik_1b} - r'_{34} r_{7-4}} t'_{45} \frac{e^{-ik_2a}}{e^{-2ik_2a} - r'_{45} r_{7-5}} t'_{56} \frac{e^{-ik_1c}}{e^{-2ik_1c} - r'_{56} r_{67}} t'_{67} \\
& + t_{67} \frac{e^{-ik_1c}}{e^{-2ik_1c} - r'_{56} r_{67}} t_{56} \frac{e^{-ik_2a}}{e^{-2ik_2a} - r'_{45} r_{7-5}} t_{45} \frac{e^{-ik_1b}}{e^{-2ik_1b} - r'_{34} r_{7-4}} t_{34} \frac{e^{-ik_2a}}{e^{-2ik_2a} - r'_{23} r_{7-3}} \\
& \times t_{23} \frac{1}{e^{-2ik_1c} - r'_{12} r_{7-2}} r'_{12} t'_{23} \frac{e^{-ik_2a}}{e^{-2ik_2a} - r'_{23} r_{7-3}} t'_{34} \frac{e^{-ik_1b}}{e^{-2ik_1b} - r'_{34} r_{7-4}} t'_{45} \frac{e^{-ik_2a}}{e^{-2ik_2a} - r'_{45} r_{7-5}} t'_{56} \frac{e^{-ik_1c}}{e^{-2ik_1c} - r'_{56} r_{67}} t'_{67}, \tag{4}
\end{aligned}$$

and

$$t' = t'_{12} \frac{e^{-ik_1 c}}{e^{-2ik_1 c} - r'_{12} r_{7-2}} t'_{23} \frac{e^{-ik_2 a}}{e^{-2ik_2 a} - r'_{23} r_{7-3}} t'_{34} \frac{e^{-ik_1 b}}{e^{-2ik_1 b} - r'_{34} r_{7-4}} t'_{45} \frac{e^{-ik_2 a}}{e^{-2ik_2 a} - r'_{45} r_{7-5}} t'_{56} \frac{e^{-ik_1 c}}{e^{-2ik_1 c} - r'_{56} r_{67}} t'_{67}. \quad (5)$$

In former equations we have used two different notations explained at the Appendix. The Hermitian case is recovered when $\gamma = 0$, thus $r = r'$ and $t = t'$ since the system has specular reflection and time reversal symmetry.

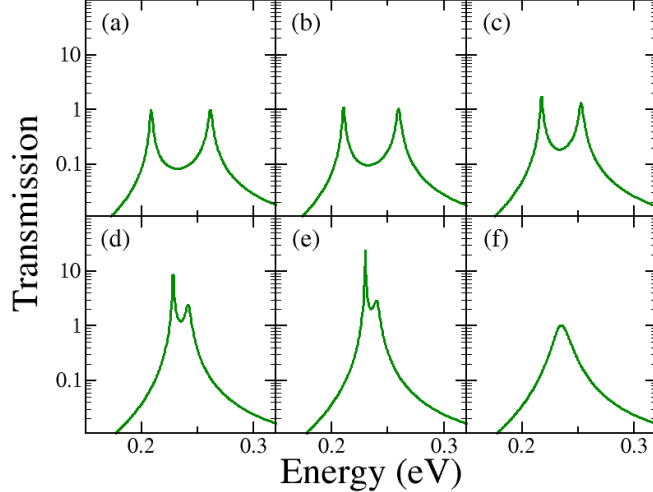


FIG. 2. Transmission spectra as a function of energy in which only the first doublet of the dimer is plotted. (a) For the Hermitian case ($\Gamma = 0$) the maximum values of the resonances are found at $E_{1,1} = 0.2086$ eV, where the first subscript refers to the associated doublet while the second one refers to the associated resonance, and $E_{1,2} = 0.2615$ eV. Dimer parameters, in this and subsequent figures, are $a = 1.15$ nm, $b = 2c = 0.02$ nm, $V_1 = 50$ eV, and $V_2 = 0$ eV. For $\Gamma = 0$ the resonances have a unit amplitude and a maximum separation. As we increase the value of Γ the separation between the resonances decreases and their amplitude increases before the EP as it is observed for Γ equal to (b) 0.010, (c) 0.020. (d) 0.026 and (e) 0.0264. For $\Gamma = 0.0264$ the resonances are already very close and overlap, losing the higher energy resonance. After the EP ($\Gamma \approx 0.0266$) the width of the resonance increases and its amplitude decreases as observed in panel (f). The same values of Γ are used in Figures 3, 4, 7, 8, and 9.

In Figure 2 the first doublet resonance spectra of the dimer is plotted as a function of energy. The resonances positions are obtained from the maxima of the total transmission ($T = |t|^2$). The Hermitian case is recovered for $\Gamma = 0$ (see panel (a)), which is related with γ through

$$\Gamma = \sqrt{\left[\frac{\hbar^2}{m} \gamma^2 + (E - V_2) \right]^2 - (E - V_2)^2},$$

and the real and immaginary part of the wavefunctions of these resonances are plotted in panel (a) of Figures 3 and 4. All the next figures are obtained when incoming waves are only from the left, *i.e.* $a_7 = 0$. As can be anticipated, the real part of the wavefunction associated to the lowest energy resonance of the doublet is a symmetric one, while the highest energy resonance is antisymmetric. On the one hand, as we increase the Γ value, the separation between the resonances decreases until they coalesce, as well as the width of the resulting resonance increases (see panels (b), (c), (d) and (e) of Figure 2). Also, the amplitude of the resonances increases but after passing the EP it starts decreasing its height (see Figure 2 (f)). This is notable since the amplitude of the resulting resonance is expected to grow indefinitely. On the other hand, as we increase Γ , the amplitude of the real and immaginary part of the wavefunction also increases. As can be seen in panels (b)-(e) of Figures 3 and 4, the amplitudes of the symmetric and antisymmetric modes grow although that of the symmetric mode grows more than the antisymmetric one. After passing the EP, in addition to the broken \mathcal{PT} -symmetry, both modes have coalesced into a mode that is neither symmetric nor antisymmetric. In fact, both modes coexist simultaneously and one is the complex conjugate of the other one. Figure 5 shows the behavior of the real and immaginary part of the energy as a function of Γ . The real part is associated with the position of the maxima of each resonance, while the immaginary part is associated with their width. The result given by the Tight Binding model predicts a decay in the separation between the eigenenergies of the system as a square root^{4,6}. In Figure 6 it is shown the fit of the difference of the resonances as a function of Γ . In purple solid line the separation between the real parts of the resonances is plotted; the yellow solid line is a pure square root while the green solid line is the best fit that was obtained from data showing a power of 0.47.

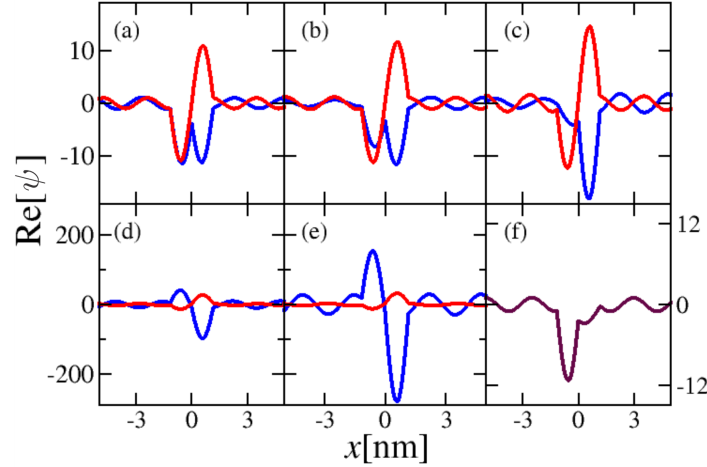


FIG. 3. Evolution of the real part ($\text{Re}[\psi]$) of the states associated to the resonances of the first doublet energy as the parameter Γ is increased. The lowest energy resonance is plotted in blue while the one with highest energy is plotted in red, panels (a) to (e). The blue wavefunctions correspond to the symmetric state while the red ones are the antisymmetric states. Once the EP is reached only one resonance remains, therefore there is only one wave function as is shown in purple in panel (f). This mode is not symmetric nor antisymmetric. Before reaching the EP, the amplitude of the wave functions also increases until it decreases once the EP is passed.

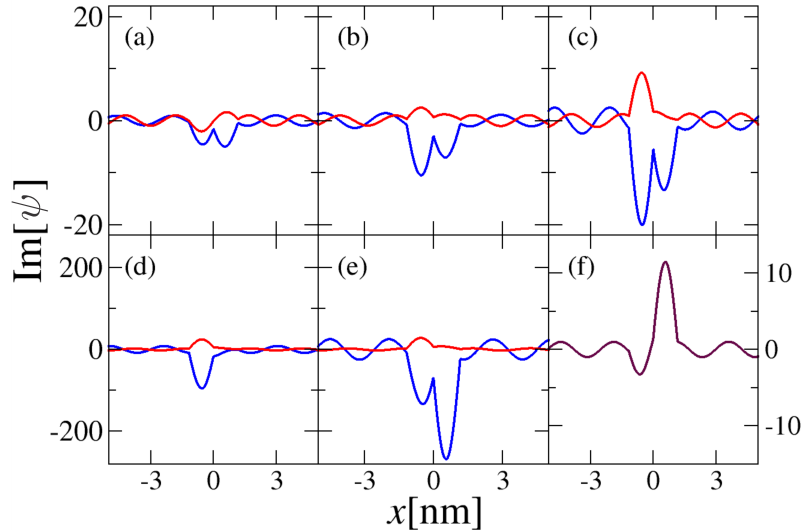


FIG. 4. Evolution of the imaginary parts of the wavefunctions ($\text{Im}[\psi]$) associated to the resonances of Figure 2. The blue, red, curve is the imaginary part of the lowest, highest, energy resonance. As in the real part, also the amplitudes increase as a function of Γ . Once the EP is passed there is only one resonance and the amplitude of the imaginary part of its wavefunction decreases as well as the real part.

III. PHASE DISTRIBUTION OF THE SCATTERING MATRIX

Now let us study the real and imaginary part of the phase as a function of the energy, the phase in Argand plane, and the phase distribution as a function of Γ .

The scattering matrix formalism allows to us to study not only the transmission and reflection amplitudes but also

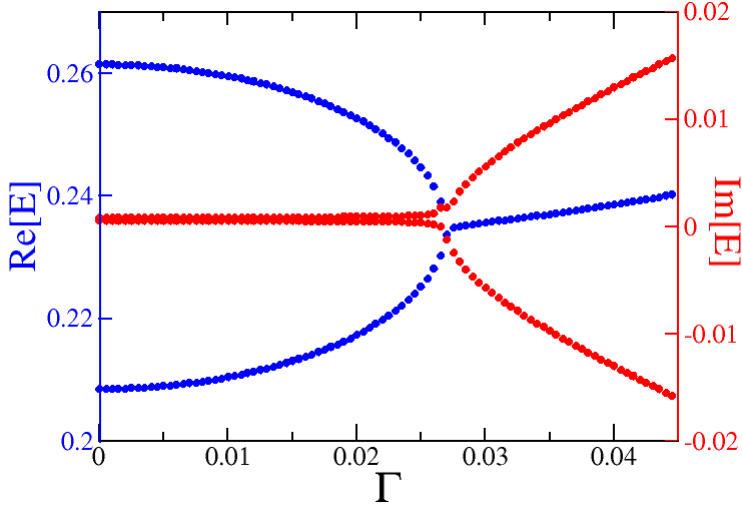


FIG. 5. EP of the dimmer. On the one hand, the real part corresponds to the positions of the resonances. For the Hermitian case, the separation of the resonances is given by the natural level repulsion. As Γ increases, the separation between the resonances decreases until both coalesce at the EP. After the EP there is only one resonance since both have coalesced. On the other hand, the imaginary part corresponds to the widths of the resonances, measured by means of the Q factor. As we get closer to the EP, the resonances overlap increasing their widths until they coalesce into a single one increasing significantly its width.

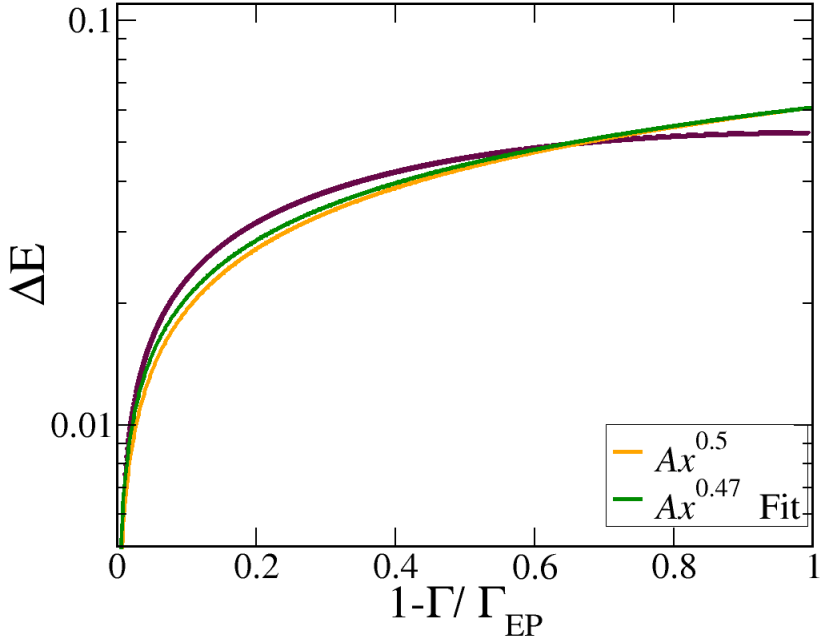


FIG. 6. The separation of the resonances as a function of Γ is shown in purple. This is compared with the fit obtained, in green, which corresponds to the model $y = Ax^B$, where $A = 0.061$ and $B = 0.47$, the latter being the power obtained that is close to the square root predicted by the tight binding model, plotted in yellow.

the phases of the system. The eigenphases of the S matrix, given after diagonalizing Eq. 1²², are

$$\begin{bmatrix} e^{i\theta} & 0 \\ 0 & e^{i\theta'} \end{bmatrix} = \begin{bmatrix} \frac{1}{2} \left(r + r' + \sqrt{(r - r')^2 + 4tt'} \right) & 0 \\ 0 & \frac{1}{2} \left(r + r' - \sqrt{(r - r')^2 + 4tt'} \right) \end{bmatrix}. \quad (6)$$

In general the eigenphases are complex and can be written as

$$\theta = \theta_{\text{Re}} + i\theta_{\text{Im}}, \quad (7)$$

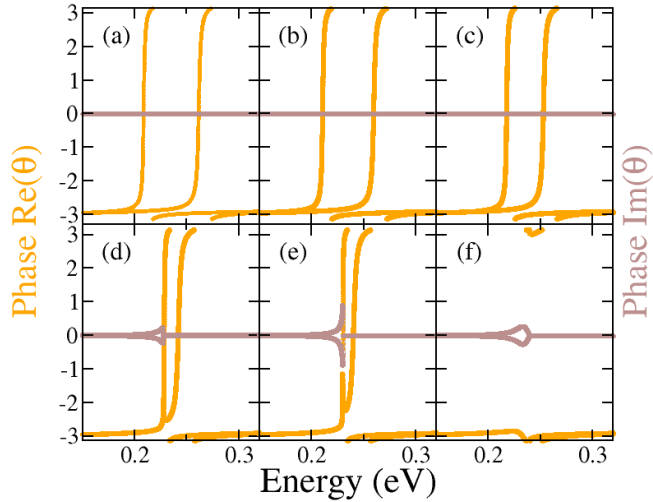


FIG. 7. Behaviour of the real (yellow solid line) and imaginary (brown solid line) parts of the phases θ and θ' as a function of the energy. (a) In the Hermitian case the separation of the resonances is maximum and the imaginary part of the phase is zero. As Γ grows the separation of the resonances diminishes (panels (b) and (c)). (d) When we approach to the EP the imaginary part stops being null and a protuberance appears near the lowest energy resonance. (e) The closer we get to the EP the more the protuberance grows. (f) Once we pass the EP, the real part of the phases lives only in the neighborhood of $-\pi$ and π , and the protuberance becomes smaller.

where θ_{Re} is the real part of the phase, while θ_{Im} is its imaginary part. Accordingly, when separating the real and imaginary part of $e^{i\theta}$ we have

$$e^{i\theta} = e^{i(\theta_{\text{Re}} + i\theta_{\text{Im}})} = e^{i\theta_{\text{Re}}} e^{-\theta_{\text{Im}}}. \quad (8)$$

The former equation can be interpreted as a module multiplied by a complex number of unitary magnitude. In other words, $e^{i\theta_{\text{Re}}}$ is a unitary complex number that, by varying the energy E , forms a circle in the Argand plane, while $e^{-\theta_{\text{Im}}}$ acts as the module of the circle.

In Figure 7 we plot the real and the imaginary part of the phase as a function of the energy. Panel (a) corresponds to the Hermitian case in which the real part has two separated resonances that correspond to θ and θ' . In this case the imaginary part is null. As Γ increases the distance between resonances becomes smaller but the imaginary part still remains zero as can be seen in panels (b) and (c). In panel (d) the resonances overlap and the imaginary part becomes not null for positive and negative values. This protuberance appears near the lowest energy resonance, which is the one that prevails. As we approach the EP the separation of the resonances reduces while the protuberance grows (panel (e)). Once the EP value has been exceeded the real part of the phase is restricted to values close to $-\pi$ and π and the imaginary part remains not null in the neighborhood of the remaining resonance as is plotted in panel (f).

Figure 8 shows the phase of both resonances in Argand plane. Blue points are the lowest energy resonance while red points are the highest energy resonance. In panels (a), (b), and (c) all of the points of each resonance are distributed in the unit circle since the imaginary part is equal to zero. In panel (d) the protuberance of the imaginary part makes that a lobe appears in the lowest energy resonance whereas that the highest energy resonance stops filling completely the circle. As the Γ value is increased even more, the lobe increases its size as does the empty space of the resonance (see panel (e)). In fact, the size of the lobe increases up to infinity and changes its concavity past the EP to reduce its size again. For its part, the distribution of the phase of the other resonance ceases to be distributed over the entire circle until only a small arc remains as can be seen in panel (f) where only one resonance remains.

Finally, in Figure 9 the histogram of the phase distribution of the two resonances under study between $-\pi$ and π is shown. The histogram in blue corresponds to the resonance with the lowest energy, also in blue, while the histogram in red corresponds to the resonance with the highest energy, also in red (see Figure 8). When the phase is distributed over the circle, in the Argand plane, its distribution takes values in the entire range from $-\pi$ to π (panels (a), (b), and (c)). When the lobe appears, as well as the empty space, this distribution changes starting to create holes (panels (d) and (e)). These gaps in the distributions grow until the histograms overlap into only one (the resonances have already coalesced) resulting in a distribution of points close to the neighborhoods of the $-\pi$ and π values shown in panel (f) (purple).

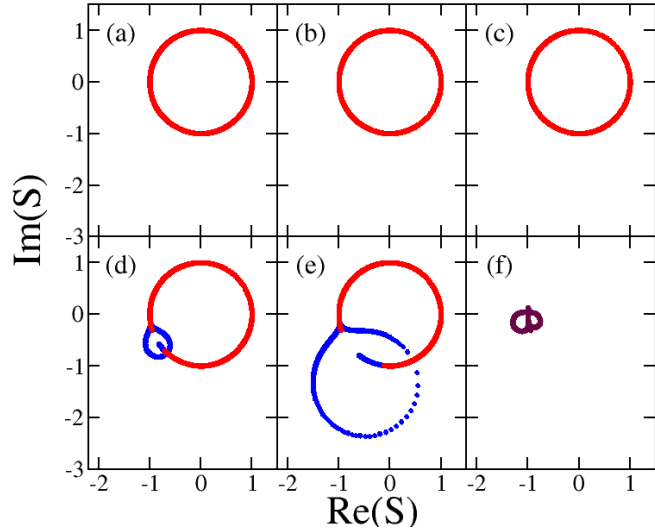


FIG. 8. Phase distribution of both resonances in Argand plane. Blue points corresponds to the lowest energy resonance while the red ones corresponds to the highest energy resonance. In (a), (b), and (c) all the points live in the unit circle because $\theta_{\text{Im}} = 0$ (blue points are below the red ones). In panels (d) and (e) the red resonance still lives in the unit circle but a lobe appears in the lowest energy resonance. This lobe increases its size up to infinity where it changes its concavity to reduce its size as Γ keeps growing. In panel (f) the coalesced resonance has diminished its size and distribution.

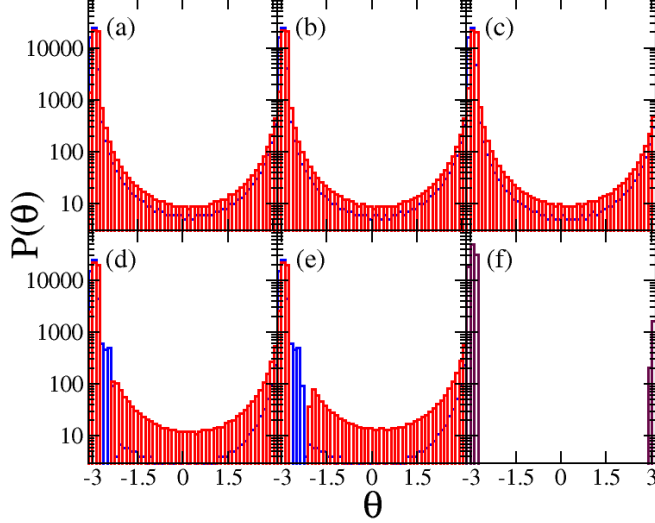


FIG. 9. Histogram of the phase distribution of the resonances as a function of Γ . Blue (red) histogram corresponds to the lowest (highest) energy resonance, except for the coalesced resonance plotted in purple. As can be inferred for Argand plane, the phases are distributed all over the angles but not in a uniform way as is shown in (a), (b) and (c). When the lobe appears the resonances stop visiting all the angles so empty spaces appear in the distribution (panels (d) and (e)). In (f) all of the points are distributed only around $-\pi$ and π .

IV. CONCLUSIONS

In this paper we have studied a quantum system in one dimension in which electrons, described by plane waves, had sent. In particular, the system that was studied consists of a dimer made up of two scatterers that presented losses and gains, parameterized by Γ . Electrons were incident on the dimer and this was described by means of the scattering matrix formalism. The S matrix provided us with the transmission coefficient from which the resonances of the system were obtained. The transmission spectrum was studied as a function of Γ and the coalescence of the resonances associated with the first doublet was observed, thus obtaining an Exceptional Point. It was observed that the separation between the resonances decays as a power as Γ increases, and when making the fit we obtained that

the power is basically a square root. Analytic expressions were developed for the elements of the scattering matrix in the non-Hermitian case.

Once the EP was obtained, we analyze the properties of the system such as the wave functions, the resonances, and the phase, before and after the EP. In the diagram of the phase against the energy we observe that before the EP the phases are separated and as we increase Γ they join; close to the EP the real part of the phase breaks while the imaginary part presents a lobe that increases its size; after the EP the phase only exists in values close to $-\pi$ and π . For the Argand plane case before the EP, we observed that initially each resonance formed a unit circle; near the EP the circles began to have a redistribution of points, while a lobe arose. This lobe increased in size significantly near the EP and once reached, the size of the lobe decreased. All the numerical evidence that we analyze suggests a saturation process that comes from inducing gains in the system. In the phase histogram the distribution of points changed as we reached the EP. Initially the points were distributed in the entire range between $-\pi$ and π , and this changed drastically when we approached the EP, firstly, appearing gaps in the distribution and then increasing the size of the empty regions as we reach the EP. After the EP the points were redistributed only around $-\pi$ and π .

ACKNOWLEDGMENTS

J. C.-G. thanks financial support from CONAHCyT. V. D.-R is grateful with the Sistema Nacional de Investigadores, Mexico, and with E. Michel-Hernández and G. T. Domínguez-Michel for their encouragement. G. B. and V. D.-R. thank financial support for the CONAHCyT project CB2017-2018/A1-S-33920 and the UAM-Azc project CB004-22.

V. APPENDIX

A. S matrix building process

The first notation uses two joined subscripts. For example, in $r'_{\eta\delta}$ we refer to the reflection that occurs between the adjacent potentials η and δ when waves incide from the right. The scattering matrix of this case is given by

$$S_{\delta\eta} = \begin{bmatrix} r_{\delta\eta} & t'_{\delta\eta} \\ t_{\delta\eta} & r'_{\delta\eta} \end{bmatrix} = \begin{bmatrix} \frac{k_\delta - k_\eta}{k_\delta + k_\eta} & \frac{2k_\eta}{k_\delta + k_\eta} \\ \frac{2k_\delta}{k_\delta + k_\eta} & -\frac{k_\delta - k_\eta}{k_\delta + k_\eta} \end{bmatrix}, \quad (9)$$

where k_δ and k_η are the wave numbers of the region δ and η , respectively. Also, $S_{\delta\eta}$ represents the scatterer between the δ and η regions.

The second notation uses two subscripts separated by a hyphen. Combinating the scattering matrices $S_{\delta\eta}$ and $S_{\eta\omega}$ gives $S_{\delta-\omega}$. For example, $t_{\delta-\omega}$ refers to the total transmission generated when the waves are transmitted from region δ to the non-contiguos region ω when incident waves arrive from the left. Part of the wave incident from the left on the scatterer $S_{\delta\eta}$ is reflected in the region δ and the other part is transmitted towards the region η . The part that was transmitted travels to the scatterer $S_{\eta\omega}$, gaining a phase in this path, in which a fraction of that wave is reflected in the region η and the other is transmitted towards the region ω . The wave that was reflected travels again to the scatterer $S_{\delta\eta}$ in which a part of that wave is reflected again into the region η and the other part is transmitted to the region δ . This process of multiple reflections in the region η is repeated infinitely. On the one hand, the sum of all the waves in the region ω is a geometric series and results in $t_{\delta-\omega}$. On the other hand, the sum of the waves in the region δ , which is also a geometric series, gives us $r_{\delta-\omega}$. These two elements are the transmission and reflection coefficients, when waves are incident from the left, of the matrix

$$S_{\delta-\omega} = \begin{bmatrix} r_{\delta-\omega} & t'_{\delta-\omega} \\ t_{\delta-\omega} & r'_{\delta-\omega} \end{bmatrix} = \begin{bmatrix} r_{\delta\eta} + t'_{\delta\eta} \frac{1}{e^{-2ik_\eta d} - r'_{\delta\eta} r_{\eta\omega}} r_{\eta\omega} t_{\delta\eta} & t'_{\delta\eta} \frac{e^{-ik_\eta d}}{e^{-2ik_\eta d} - r'_{\delta\eta} r_{\eta\omega}} t'_{\eta\omega} \\ t_{\eta\omega} \frac{e^{-ik_\eta d}}{e^{-2ik_\eta d} - r'_{\delta\eta} r_{\eta\omega}} t_{\delta\eta} & r'_{\eta\omega} + t_{\eta\omega} \frac{1}{e^{-2ik_\eta d} - r'_{\delta\eta} r_{\eta\omega}} r'_{\delta\eta} t'_{\eta\omega} \end{bmatrix}.$$

This procedure is also valid if it is necessary to build the system from the right since $S = S_{1-7} = S_{7-1}$. In particular, this combination procedure is performed five times for the dimer by adding potential barriers from left to right. A

part of the analytical expression of the reflection coefficient (Equation 2) of the dimer is

$$\begin{aligned}
 r = & r_{12} \\
 & + t'_{12} \frac{1}{e^{-2ik_1c} - r'_{12} r_{23}} r_{23} t_{12} \\
 & + t'_{12} \frac{e^{-ik_1c}}{e^{-2ik_1c} - r'_{12} r_{23}} t'_{23} \frac{1}{e^{-2ik_2a} - r'_{1-3} r_{34}} r_{34} t_{23} \frac{e^{-ik_1c}}{e^{-2ik_1c} - r'_{12} r_{23}} t_{12} + \dots
 \end{aligned} \tag{10}$$

Here r_{12} is the reflection that occurs when waves are incident from the left on the boundary between region I and region II. The second term of r represents the wave that was transmitted from region I to region II, it suffers a process of multiple reflections between regions II and III, and was transmitted from region II to region I. The third term represents the wave that was transmitted from region I to region II, it suffers a process of multiple reflections between the boundaries of region II, was transmitted from region II to region III, was reflected multiple times between the boundaries of region I and region IV (note the term r'_{1-3} in the denominator), was transmitted from region III to region II, reflected multiple times in region II, and was finally transmitted from region II to region I. The physical interpretation continues in the same way for subsequent terms. The interpretation of the transmission coefficient follows a process equivalent to that of r .

* colinlug05@gmail.com

† ele@xanum.uam.mx

‡ gbaez@azc.uam.mx

§ vdr@azc.uam.mx

- ¹ C. M. Bender and S. Boettcher, “Real spectra in nonhermitian hamiltonians having \mathcal{PT} symmetry”, PRL **80**, 5243 (1998)
- ² C. M. Bender, D. C. Brody and H. F. Jones, “Complex extension of quantum mechanics”, PRL **89**, 270401 (2002)
- ³ C. M. Bender, “Making sense of non-Hermitian Hamiltonians”, Rep. Prog. Phys. **70**, 947 (2007)
- ⁴ T. Kato, “Perturbation Theory for Linear Operators”, Springer-Verlag, Berlin, (1966), pp. 63–64
- ⁵ A. Krasnok, N. Nefedkin and A. Alu, “Parity-Time Symmetry and Exceptional points: A Tutorial” Optica Open. Preprint. <https://doi.org/10.48550/arXiv.2103.08135> (2021)
- ⁶ W. D. Heiss, “The physics of exceptional points”, J. Phys. A: Math. Theor. **45**, 444016 (2012)
- ⁷ T. T. Koutserimpas, and F. Romain. “Electromagnetic fields in a time-varying medium: exceptional points and operator symmetries.” IEEE Transactions on Antennas and Propagation **68**, 9 (2020)
- ⁸ H. Hodaei, AU. Hassan, S. Wittek and H. Garcia-Garcia. “Enhanced sensitivity at higher-order exceptional points.” Nature **548**, 7666 (2017)
- ⁹ C. Shi, M. Dubois, Y. Chen, L. Cheng, H. Ramezani, Y. Wang, and X. Zhang. “Accessing the exceptional points of parity-time symmetric acoustics”, Nat. Commun. **7**, 11110 (2016)
- ¹⁰ S. K. Özdemir, S. Rotter, F. Nori, and L. Yang. “Parity-time symmetry and exceptional points in photonics”. Nature materials, **18**, 8 (2019)
- ¹¹ V. Domínguez-Rocha, Ramathasan Thevamaran, F.M. Ellis and T. Kottos, “Environmentally Induced Exceptional Points in Elastodynamics”, Phys. Rev. Applied **13**, 014060 (2020)
- ¹² S. Longhi. “Quantum interference and exceptional points”. Optics Letters **43**, 21 (2018)
- ¹³ S. Assawaworrarit, X. Y. Xiaofang, and S. Fan. “Robust wireless power transfer using a nonlinear parity-time-symmetric circuit”. Nature **546**, 7658 (2017)
- ¹⁴ H. Cartarius, J. Main, and G. Wunner. “Exceptional points in atomic spectra”. Phys. Rev. Letters **99**, 17 (2007)
- ¹⁵ B. Zhen, C. W . Hsu, Y. Igarashi, L. Lu, I Kaminer, A. Pick and M. Soljačić. “Spawning rings of exceptional points out of Dirac cones”. Nature **525**, 7569 (2015)
- ¹⁶ Y. V. Kartashov, C. Millán, V. V. Konotop and L. Torner. “Bound states in the continuum in a two-dimensional PT-symmetric system”. Optics letters **43**, 3 (2018)
- ¹⁷ R. Kononchuk, J. Cai, F. Ellis, Ramathasan Thevamaran and T. Kottos. “Exceptional-point-based accelerometers with enhanced signal-to-noise ratio”. Nature **607**, 697 (2022)
- ¹⁸ P. Pereyra, “Fundamentals of Quantum Physics” (Springer Science and Business Media, 2012) chapters 4, 5 and 7
- ¹⁹ P. A. Mello and N. Kumar, “Quantum Transport in Mesoscopic Systems: Complexity and Statistical Fluctuations” (Oxford University Press, New York, 2005), chapters 2 and 3
- ²⁰ N. Moiseyev, “Non-Hermitian Quantum Mechanics” (Cambridge University Press, UK, 2011), chapters 1 and 2
- ²¹ D. Ferry, S. Marshall. “Transport in Nanostructures” (Cambridge University Press, 1999), chapters 3 and 4
- ²² M. Martínez-Mares, A. Robledo. “Equivalence between the mobility edge of electronic transport on disorderless networks and the onset of chaos via intermittency in deterministic maps”. Phys. Rev. E **80**, 4 (2009)